Journal of Environmental Management 341 (2023) 118031

Contents lists available at ScienceDirect

Journal of Environmental Management

journal homepage: www.elsevier.com/locate/jenvman

Research article

Removal of NO at low concentrations from polluted air in semi-closed environments by activated biochars from renewables feedstocks

Carlos G. Díaz-Maroto [a,b], Ondřej Mašek [c], Patricia Pizarro [a,b], David P. Serrano [a,b], Inés Moreno [a,b], Javier Fermoso [a,*]

[a] Thermochemical Processes Unit, IMDEA Energy, Avda. Ramón de la Sagra 3, 28935, Móstoles, Madrid, Spain
[b] Chemical and Environmental Engineering Group, Rey Juan Carlos University, Móstoles, Madrid, Spain
[c] UK Biochar Research Centre, School of Geosciences, University of Edinburgh, Crew Building, Alexander Crum Brown Road, Edinburgh, EH9 3FF, UK

ARTICLE INFO

Keywords:
Polluted air
Activated carbon
Carbonaceous catalysts
Low concentration NO
NO oxidation
NOx elimination

ABSTRACT

Efficient measures are urgently required in large cities for nitric oxide (NO) elimination from air in urban semi-closed environments (parking lots and tunnels), characterized by low NO concentrations (<10 ppmv) and temperatures. One of the most promising abatement alternatives is the NO oxidation to NO_2, which can be further easily captured in an alkali solution or over a porous solid. However, most of the research devoted to this topic is focused on the elimination of NO from fuel exhaust gases, with high NO concentrations (400–2000 ppmv). In this work, sustainable and low-cost activated biochars of different origin and having very different ash contents were employed in NO removal at very low concentrations. Thus, low ash content forestry (oak woodchips, OAK) and high ash content from agriculture (oilseed rape straw, OSR) biochars were subjected to physical activation with CO_2 at 900 °C (OAK550-A900CO_2 and OSR700-A900CO_2, respectively). The NO removal performance tests of such activated carbons were carried out at different experimental conditions: i.e., temperature, relative humidity (0–50 vol% RH), NO-containing gas (N_2 or air), amount of activated carbon, and NO concentration, to assess how the activated biochar properties influence their NO removal capacity. The sample OSR700-A900CO_2 contained a higher population of oxygen surface functionalities, which might play an important role in the NO removal efficiency in dry conditions since they could assist NO oxidation on carbon active sites when used above room temperature (50–75 °C). However, at room temperature (25 °C), the presence of narrow micropore size distribution at 6 Å became a more relevant property, since it facilitates an intimate contact between NO and O_2. Accordingly, the activated biochar from OAK was much more efficient, achieving complete removal of NO from air flow (dry or with 50 vol% RH) at 25 °C during 400 min of testing, making it an ideal candidate as biofilter for purifying air streams of semi-closed spaces contaminated with low concentrations of NO.

1. Introduction

Anthropogenic nitrogen oxides (NOx) are considered important atmospheric pollutants as they are the main precursors of negative environmental impacts, such as acid rain and photochemical smog, causing severe harmful effects on human health. These issues are particularly severe in large cities as a consequence of the increasing road transport due to the huge growth of population and standard of living in urban areas (Shaw and Van Heyst, 2022; Wang et al., 2015). Therefore, more stringent restrictions have been imposed by most of the authorities in developed countries. For instance, the European Ambient Air Quality Directive established more restrictive NOx concentrations thresholds, setting hourly and yearly limit values of 200 and 40 μg/m^3, respectively (Derwent and Hjellbrekke, 2019). However, these air quality standards are particularly difficult to achieve in those semi-closed environments (road tunnels and parking lots), where there is generally low ventilation efficiency and automobile exhaust emissions are concentrated, causing the risk of health problems (Demir, 2015). In particular, in such located spaces, the concentration of NOx usually is very low, reaching values up to 10 ppmv, containing approximately 90% nitric oxide (NO) (Pan et al., 2017). This is a much lower concentration than the typical considered in most studies regarding the treatment of NOx-contaminated gases. This

* Corresponding author.
E-mail address: javier.fermoso@imdea.org (J. Fermoso).

https://doi.org/10.1016/j.jenvman.2023.118031
Received 23 December 2022; Received in revised form 9 March 2023; Accepted 25 April 2023
Available online 9 May 2023

fact, along with the ambient air conditions in such spaces (low temperature and variable relative humidity) makes particularly challenging any de-NOx in-situ application.

Selective Catalytic Reduction (SCR) is the most widely used technology for the abatement of NO emissions in flue gas effluents produced by stationary sources (Feng et al., 2022; Gui et al., 2022). In the case of mobile sources, SCR is also a mature process for diesel vehicles; whereas, for gasoline engines, NO emissions can be effectively controlled with three-way catalysts (TWCs). However, these systems are only effective for high NO concentrations, operating at high temperatures (300–400 °C), oxygen concentrations close to stoichiometric combustion, and require the utilization of expensive metal-based catalysts (Brandenberger et al., 2008). Accordingly, these technologies are not appropriate for NOx removal in semi-closed spaces, mainly characterized by a low NOx concentration under ambient conditions (relatively low temperatures and high oxygen concentration).

As an alternative, NO catalytic oxidation is considered a highly-effective option for NO removal at low temperatures (<100 °C). At high concentrations, NO is very reactive with oxygen, yielding NO_2, which can be subsequently captured in an aqueous solution or easily adsorbed on porous solids (Hong et al., 2017; Shen et al., 2016). However, at values lower than 1000 ppmv, NO is very stable, hindering its oxidative removal in air and requiring the use of highly active catalysts (Mochida et al., 1994, 1997). Carbonaceous solids (activated carbons, CNFs, CNTs, graphene oxides, xerogels, etc.) provide numerous benefits as low-temperature NO oxidation catalysts, such as their excellent catalytic performance at room temperature and low energy requirements (Anthonysamy et al., 2022; Deng et al., 2020; Silas et al., 2019).

Lignocellulosic precursors, such as pyrolysis biochars, have been widely used as low-cost and renewable raw materials to prepare active carbons for a wide range of applications as adsorbents and catalysts (Azargohar and Dalai, 2006; Nor et al., 2013). Both physical (CO_2 and steam) and chemical processes (KOH, K_2CO_3, HNO_3, etc) can be applied to provide biochars with different textural and chemical properties. The activation conditions (temperature, time, and gasifying or chemical reagents employed), as well as the nature of the raw biomass used as feedstock, are the main factors influencing the final properties of the activated biochars (Gwenzi et al., 2021; Jeguirim et al., 2018; Kalinke et al., 2017; Qu et al., 2021; Siipola et al., 2018).

Nonetheless, despite the huge potential presented by those carbon materials, the reaction mechanism and the carbon characteristics that promote the oxidation process are not completely elucidated (Deng et al., 2020; Qiu et al., 2009; Valenciano et al., 2015). Thus, Zhang et al. investigated NO oxidation over a variety of active carbons with different textural properties concluding that NO_2 formation is favoured by the presence of narrow micropores (~6–7 Å), which provide very close contact between NO and O_2, not being influenced by the overall surface area neither by the chemical properties (Zhang et al., 2008). The presence of oxygenated and nitrogen surface groups are also relevant features for the NO oxidation process since they affect the kinetics of NO/NO_2 adsorption-desorption, increasing the rate of NO oxidation (Adapa et al., 2006; Atkinson et al., 2013). In this regard, recently, Wang et al. described that the presence of small traces of potassium in coal-derived carbons prepared by hydrothermal activation with K_2CO_3 might promote the formation of oxygenated functional groups (C–O) when these were subjected to a simulated flue gas containing oxygen, resulting in an improved removal of low concentration NO at 50 °C (Wang et al., 2022). However, it is important to highlight that most of the works devoted to this topic investigated the NOx removal capacity of carbonaceous solids, with different physicochemical properties, from gaseous streams at high NOx concentrations (200–2000 ppmv) and relatively low temperatures (30–50 °C). Conversely, there are hardly any works in the scientific literature focused on the particular application of carbonaceous solids in the NOx abatement at low concentrations (<10 ppm) (G. Diaz-Maroto et al., 2023; Ghouma et al., 2017; Wang et al., 2011) as are those usually found in semi-closed spaces of urban areas. This issue is considered a great challenge because of the scarce reactivity of NO when it is found at very low concentrations and low temperatures. Ghouma et al. (2017) evaluated the performance of agro-industrial derived carbons on the NO_2 removal at a concentration of 5 ppmv and 23 °C, but not on the NO elimination. However, unlike NO, NO_2 shows a high affinity to be adsorbed on the surface of porous solids. On the other hand, Wang et al. prepared Porous Carbon Nanofibers (PCNFs) derived from synthetic Polyacrylonitrile (PAN) fibres, which were able to remove up to 60 or 100% of NO, depending on the NO inlet concentration (2 and 20 ppm, respectively) at 30 °C (Wang et al., 2011). Alternatively, there are also a very limited number of works, in which metal oxides (e.g MnOx, Mg-doped MnOx or Fe/Mn binary oxides) have been tested under experimental conditions (10 ppm NO and room temperature), similar to those of semi-closed urban spaces, giving 100% NO removal efficiency (Pan et al., 2017; Shu et al., 2013; Wang et al., 2015).

Nevertheless, in a recent work, we investigated the effect of physical activation conditions (temperature, activating agent) on the NO removal efficiency using a pyrolysis biochar as carbon precursor, with which we achieved the total NO removal (5 ppmv) from a gas flow (with > 5 vol% O_2) (G. Diaz-Maroto et al., 2023).

In this context, the main novelty and motivation of this work are to investigate the behavior on the NO removal at low concentrations and temperatures using low-cost and renewable activated carbons obtained from the activation of biochars, obtained as by-product in two kinds of pyrolysis reactors operating under different experimental conditions to produce bio-oil (as main product) for biofuels or biochemical applications. Two residues with very different origin and ash content, oak (OAK550) and oilseed rape straw (OSR700), were used as feedstocks. The biochars were physically activated with CO_2 and evaluated as NO retention filters simulating the air conditions found in semi-closed and low-ventilated urban spaces (e.g., road tunnels or parking lots), having low NO concentration (2.5–7.5 ppmv) and low-moderate temperatures (25–75 °C). Special attention has been paid to the role of textural properties and surface chemistry in NO removal.

2. Materials and methods

2.1. Materials

In this study, two biomass residues with diverse origin (forest and agricultural), ash content and pyrolysed in two kinds of reactors operated under different experimental conditions, were selected as carbonaceous precursors to produce activated carbons and compare their NO removal capacity from polluted gaseous streams. On the one hand, oak woodchips, in form of small particles 1–2 mm of diameter, was pyrolysed at 550 °C, with a heating rate of 10 °C/min and a N_2 total flow rate of 4 L/min with a residence time of 60 min in a fixed-bed reactor, producing a biochar yield of 17 wt%, named OAK550. On the other hand, oilseed rape straw (OSR), in form of pellets with an average size of 10 mm length and 5 mm diameter, was pyrolysed at 700 °C, with a heating rate of 100 °C/min and a biomass residence of time of 12 min in a rotatory kiln reactor, giving rise to a biochar yield of 23 wt%, named OSR700 (Mašek et al., 2018).

2.2. Biochar activation

2.2.1. Physical activation: CO_2

Both OAK550 and OSR700 biochars were physically activated with CO_2 using a lab-scale setup, whose schematic diagram is represented in Fig. S1. A detailed description of the setup and the activation experimental procedure can be found in the Supplementary Material. The resulting activated carbons were denoted as OAK550-A900CO_2 and OSR700-A900CO_2, respectively.

The degree of activation or *burn-off* level was calculated according to Equation (1).

$$Burn-off\ (\mathrm{wt.\%}) = \frac{W_{0,daf} - W_{f,daf}}{W_{0,daf}} \bullet 100 \quad (1)$$

where $W_{0,daf}$ and $W_{f,daf}$ refer to the initial and final sample weight (in dry and ash free basis), respectively, during the isothermal stage at 900 °C under CO_2 flow.

2.3. Physico-chemical characterisation of samples

Proximate analysis (moisture, volatile matter, and ash contents) of raw biochars and activated carbons were determined according to European standards. Ultimate analysis (elemental composition) of biochars and activated samples was determined in a Thermo Scientific FLASH 2000 CHNS/O micro-elemental analyser, where C, H, N and S concentrations were obtained, while O concentration was calculated by difference. The ash fraction obtained from the calcination of the carbonaceous samples was analysed by Inductively Coupled Plasma-Optical Emission Spectroscopy (ICP-OES) with a PerkinElmer Optima 3300 DV instrument. Textural properties of the activated carbons were measured by N_2 and CO_2 adsorption-desorption isotherms at 77 K and 273 K, respectively, in a Micromeritics 3Flex analyser equipped with a high-vacuum system and three 0.1 Torr pressure transducers. Fourier transform infrared spectra (FT-IR) were measured in a Thermo Fisher Scientific Nicolet 6700 equipped with a ceramic source, KBr beam splitter and a DTGS detector. The existence of oxygenated surface groups in activated biochars was analysed by Temperature Programmed Desorption coupled to Mass Spectroscopy (TPD-MS) by means of monitoring the evolved CO, CO_2 and H_2O during heating treatment. All of the above techniques for the physico-chemical characterisation of the activated biochars and the corresponding experimental procedures have been described in the Supplementary Material.

2.3.1. NO removal tests from polluted air streams

The NO removal tests were carried out in a lab-scale filter, whose schematic diagram is depicted in Fig. 1. This setup consisted of a glass updraft fixed-bed column (500 mm length, 16 mm internal diameter) with a porous plate, in which the activated carbon was placed. This area was covered with a heating tape to control the temperature of the removal tests. The gas inlet stream was generated in a NO_x calibrator (Ecotech Serinus 3000) containing three gases: air (air zero generator), N_2 (99.999 vol%), and 50 ppmv NO (balance N_2). The NO_x calibrator set the inlet concentration of NO and O_2 in the gas stream, whose total flow was 1000 mL/min. The gas outlet concentrations were continuously measured with the NO_x (NO and NO_2, with a detection limit of 1 ppb) analyser Ecotech Serinus 40. However, in the course of the experiments here performed, the NO_2 concentration at the outlet of the filter remained almost invariable at negligible values. Thus, the results of the tests were represented on NO breakthrough curves, plotting C/C_0 versus time, where C and C_0 are the NO instant outlet and the inlet concentrations (ppmv), respectively.

In this study, key process conditions, such as operating temperature (25–75 °C), the presence of relative humidity (0 and 50 vol% RH) in the air stream, NO concentration ($[NO]_{in}$ = 2.5–7.5 ppmv), gas stream nature (air or nitrogen) and carbon load (1.5 and 3 g) were evaluated over the NO removal performance of the prepared materials for 400 min.

The total NO elimination capacity was calculated by Equation (2).

$$NO_{elimination}(\%) = \frac{NO_{in}(mg) - NO_{out}(mg)}{NO_{in}(mg)} \bullet 100 \quad (2)$$

where, NO_{in} and NO_{out} represent the total amount of NO (in mg) fed and remaining in the exhaust gas, respectively; and NO_i (i.e. NO_{in} and NO_{out}) was calculated by Equation (3).

$$NO_i\ (mg) = \frac{Q_{air_{in}}(mL/min) \bullet [NO]_{in}(ppmv) \cdot 1\ atm}{0.082\ \left(\frac{atm \cdot mL}{mmol \cdot K}\right) \cdot 298K} \cdot 30\ \left(\frac{mg_{NO}}{mmol_{NO}}\right) \cdot time\ (\mathrm{min}) \quad (3)$$

where: $Q_{air\ in}$ = 1000 mL/min; $[NO]_{in}$ = 2.5–7.5 ppmv and *time* = 400 min.

3. Results and discussion

3.1. Physico-chemical characterization of carbonaceous materials

Two pyrolysis biochars obtained from different biomass residues of forest (oak woodchips, OAK550) and agricultural origin (oilseed rape straw, OSR700) with very different ash content were selected as raw materials for the preparation of activated carbons via physical activation with CO_2 at 900 °C. First, both raw biochars and the corresponding activated carbons were characterized to elucidate how the properties and origin of the raw biochar can affect the physicochemical features of the final active carbon.

Table 1 presents the proximate and ultimate analyses of both raw biochars (OSR700 and OAK550) and the resulting carbons after physical activation with CO_2 at 900 °C. The *burn-off* or activation degree determined according to Equation (1) is also included.

As can be observed, both raw biochars contain a similar amount of volatile components (ca. 13.7–14 wt%, respectively). However, the

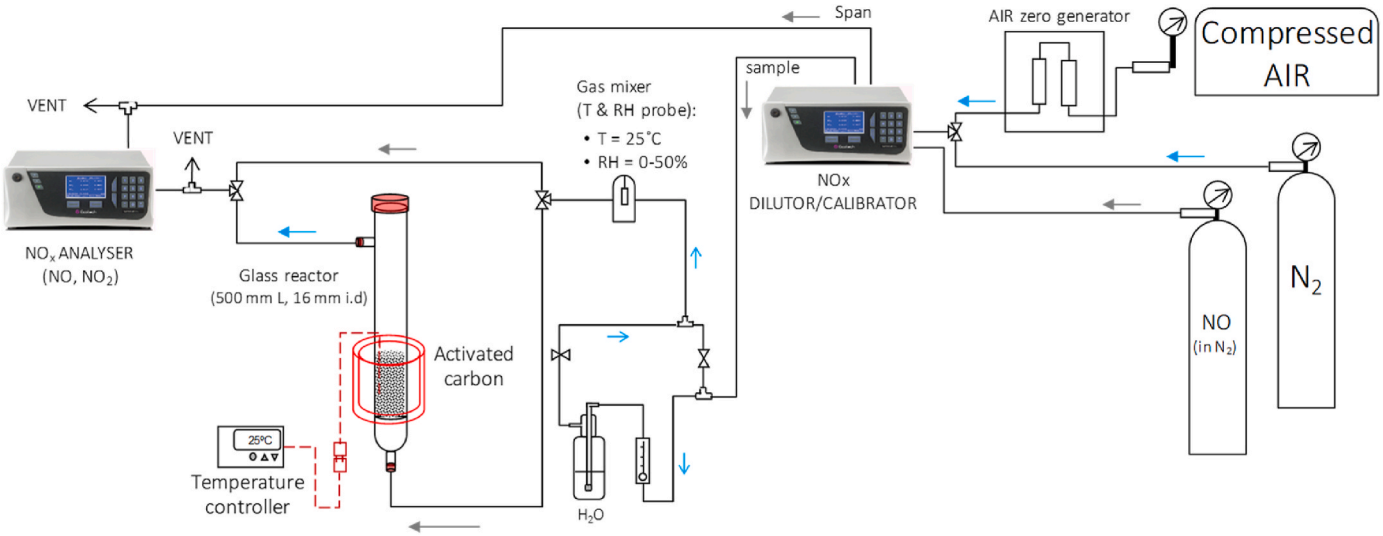

Fig. 1. Schematic diagram of the lab-scale filter to remove NO_x (NO and NO_2) from contaminated gaseous streams.

Table 1
Proximate and ultimate analysis of both raw biochars and derived activated carbons.

Sample	*Burn-off* (wt.%)	Proximate Analysis, db (wt.%)			Ultimate Analysis, daf (wt.%)				
		Volatile Matter	Ash	Fixed Carbon	C	H	N	S	O
OAK550	–	14.0	1.5	84.5	91.2	2.3	0.1	0.0	6.5
OAK550-A900CO_2	26.9	0.0	2.1	97.9	96.1	0.5	0.2	0.0	3.2
OSR700	–	13.7	22.4	63.9	87.0	1.5	1.1	0.0	10.4
OSR700-A900CO_2	30.1	0.0	32.8	67.2	91.8	0.9	1.3	0.0	6.0

db: dry basis; daf: dry and ash-free basis.

oilseed rape straw biochar (OSR700) presents a much higher ash content than that determined from the forestry residue (OAK550), that is 22.4 *vs* 1.5 wt%, respectively, which is in good agreement with the literature (Fermoso et al., 2017). Consequently, the fixed carbon percentage is significantly higher in this last sample, reaching a value of 84.5 wt%. According to the CHNS/O elemental analysis, OAK550 biochar presents significantly lower oxygen content than OSR700 (6.5 vs 10.4 wt%), which denotes a lower amount of oxygenated surface functional groups.

The volatile matter was fully removed in both activated carbons, regardless of their origin. Such elimination mainly occurred during the heating-up period under nitrogen flow, before the CO_2 activation at 900 °C stage. Then, once the activation temperature was reached, CO_2 reacts with the carbon surface, opening the porous structure of the biochar by extracting part of the carbon atoms. But the surface chemistry of the remaining carbon can be also modified since oxygenated species can be partially released due to the high activation temperature (900 °C) applied. Thus, the elemental analysis, on dry and ash-free basis, shows a C enrichment to the detriment of H and O contents (Chen et al., 2017; Zhang et al., 2014). Therefore, those activated carbons are deeply carbonized materials, being constituted mostly by aromatic structures (Hwang et al., 2017; Janu et al., 2021; Jouiad et al., 2015). After the activation process, the ash content of both samples augments proportionally to those values of the raw biochars (as they remain in the solid), according to their burn-off degree. In this regard, for OSR700-A900CO_2, this share increases significantly, from 22.4 up to 32.8 wt%, while in the case of OAK550-A900CO_2, this value varies from 1.5 to 2.1 wt%. The burn-off percentage estimated for the OSR700-A900CO_2 is somewhat higher than that determined for the OAK550-activated biochar. This difference could denote a certain catalytic effect of the mineral fraction contained in this sample, particularly rich in K (see Table 2), which may favor CO_2 gasification reactions by reducing the activation energy (Ea) during the gasification process (Hu et al., 2019).

N_2 adsorption-desorption isotherms at 77 K for both activated carbons are depicted in Fig. 2. They exhibit combined features of type I (b) and IV, according to the IUPAC classification. Thus, a strong N_2 uptake occurs at relative pressures lower than 0.1, which denotes the predominance of a well-developed microporosity. The wide "knee" curvature of the isotherm at these relative pressures indicates that this microporosity is relatively heterogeneous in size (Thommes et al., 2015; Yang et al., 2012). In addition, the progressive adsorption produced at intermediate P/P_0 values denotes the formation of a broad mesoporosity during the activation process. Both isotherms show a relatively narrow H4 hysteresis loop in the range of low-medium pressures, which is usually assigned to the presence of micropores with slit geometry.

The substantial difference observed in the N_2 volume adsorbed indicates that OAK550-A900CO_2 presents higher adsorption capacity, especially in the micropore range, than the activated carbon derived from OSR700. This variation is confirmed by the CO_2 physisorption analyses depicted in Fig. S2, which were performed to complement the analysis of the textural properties in the narrow micropore zone.

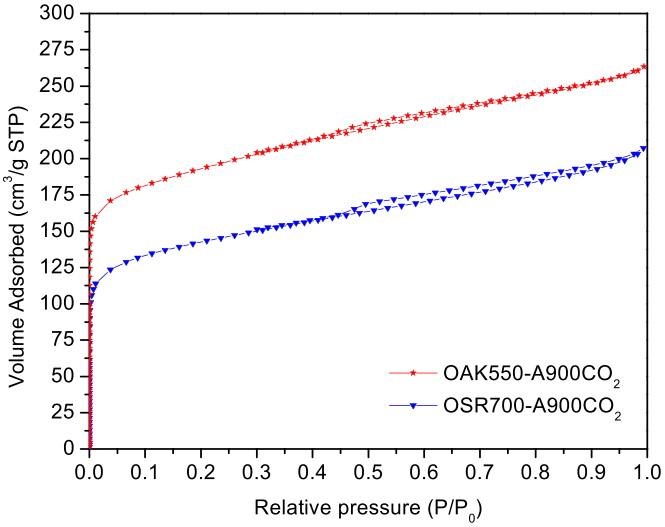

Fig. 2. N_2 adsorption-desorption isotherms at 77 K for activated carbons prepared from CO_2 activation of OAK550 and OSR700 biochars.

The values of the textural properties determined for these samples (Table 3) follow a similar trend. Thus, the S_{BET} (m^2/g_{db}) corresponding to the OAK activated biochar is higher than that of OSR700-A900CO_2. This increase is attributed to the major contribution of the microporous system, but also the external porosity (associated with both meso- and macropores) generated during the CO_2 activation process. These results can be assigned to the higher proportion of inorganic matter in OSR-

Table 3
Textural properties of the activated carbons prepared from CO_2 activation of OAK550 and OSR700 biochars (determined from N_2 isotherms).

Sample	S_{BET} (m^2/g_{db})	S_{MIC} (m^2/g_{db})	S_{EXT} (m^2/g_{db})	V_{MIC} (cm^3/g_{db})	V_{Total} (cm^3/g_{db})
OAK550-A900CO_2	723	456	267	0.18	0.397
OSR700-A900CO_2	530	346	184	0.14	0.307

S_{BET}: BET surface area; S_{MIC} (micropore surface area), S_{EXT} (external surface area) and V_{MIC} (micropore volume) calculated using the t-plot method; V_{Total}: total pore volume at $P/P_0 \approx 0.97$.

Table 2
ICP-OES analysis of activated carbons prepared from CO_2 activation of OAK550 and OSR700 biochars.

Element, db (wt.%)	Al	Ca	Fe	K	Mg	Na	P	Others (<0.1 wt%)	Ash
OAK550-A900CO_2	0.03	1.65	0.01	0.17	0.07	0.03	0.06	0.08	2.1
OSR700-A900CO_2	0.15	10.3	0.53	18.08	1.10	0.59	1.83	0.16	32.8

db: dry basis.

derived biochar, which does not show any porous structure. In fact, if the specific surface areas were estimated referred to the mass of organic matter (i.e. per gram in dry and ash free basis), the OSR700-A900CO_2 would reach a value of 788 m^2/g_{daf}, being somewhat higher than that estimated for the OAK550-activated biochar, which will show a value of 735 m^2/g_{daf}.

Through the combination of both CO_2 and N_2 isotherms, the pore size distribution (PSD) of the two activated carbons was determined by applying the model 2D-NLDFT and considering a slit pore geometry (Fig. 3). For clarity, the CO_2 isotherm is used to define the ultra-small microporosity zone (pore size < 10 Å) while the N_2 isotherm allows the estimation of the pore size distribution in the large-microporous and mesoporous range (pore size > 10 Å) (Jagiello et al., 2019). As can be observed, both samples exhibit a wide pore size distribution typical of activated carbons obtained by physical activation methods (Lozano-Castelló et al., 2004). OAK550 activated carbon presents a bimodal pore size distribution comprising a microporosity with an average diameter of 6 Å, and a secondary broad mesoporosity centred at around 37 Å. The presence of micropores around ~ 6–7 Å could be a positive feature, as this value is considered to be optimal for NO removal (Zhang et al., 2008; Zhu et al., 2022).

In contrast, in the case of OSR700-A900CO_2, the PSD reveals the existence of trimodal porous structure, showing broad microporosity with a significant contribution of micropores with sizes around 6 and 10 Å, together with a broad mesoporosity centred at 36 Å. It should be noticed that the cumulative pore volume of the micropores with an average diameter of 6 Å is much higher in OAK550-A900CO_2 than that

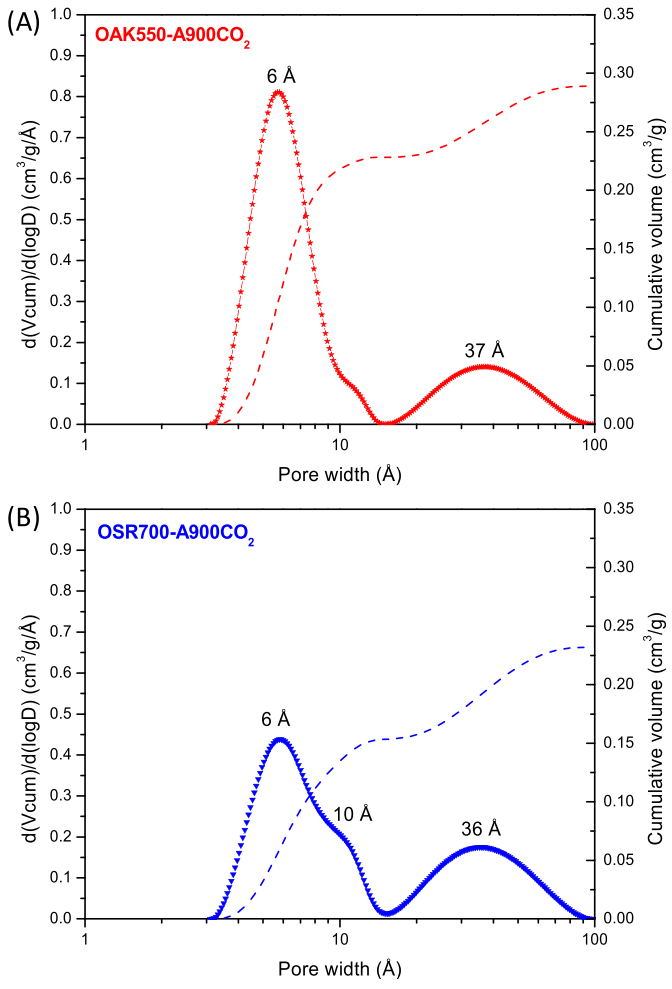

Fig. 3. 2D-NLDFT pore size distributions of the activated carbons derived from OAK550 (A) and OSR700 (B) biochars.

exhibited by OSR700-A900CO_2, showing values of 0.5 and 0.26 cm^3/g, respectively. This difference is still maintained even if it was estimated regarding the carbonaceous matter content (0.5 cm^3/g *vs* 0.39 cm^3/g) which would be indicative that OAK activated carbon has a higher proportion of micropores of this size.

Analyses of the chemical groups on the surface of activated carbons were attempted by FT-IR and TPD-MS techniques. Fig. 4 shows the FT-IR spectra for the raw biochars (A, B) and activated carbons (C, D), respectively. A higher amount of surface functionalities in OSR700 than in OAK550 is detected according to the larger intensity of the different registered bands. Of particular larger intensities are the bands appearing at wavenumbers of 750–900 cm^{-1} and 1030 cm^{-1}, assigned to the stretching of the aryl C–H and C–O bonds and the C–O and C–O–C, respectively. The O–H band at 3700 cm^{-1} is also more intense. Finally, there are also two intense peaks at 1600 cm^{-1} and 1200 cm^{-1} corresponding to the stretching vibration of the carbonyl group (C=O) and from the C–O stretching vibration of anhydride and ether groups, respectively.

The activation with CO_2 of OAK-derived biochar caused a strong reduction of the absorption bands (Fig. 4D) associated with the presence of oxygenated functional groups (Wang et al., 2022). The elimination of these surface functionalities is relatively predictable for those processes involving high operating temperatures, like physical activation with CO_2 at 900 °C. Accordingly, the chemical groups present on the carbon surface are partially removed due to bonding destruction and self-cracking reactions (Armynah et al., 2019; Barroso-Bogeat et al., 2019; Lu et al., 2017). However, after the activation process, OSR700-A900CO_2 preserves almost all the oxygenated functional groups on the surface according to the corresponding FT-IR spectrum, which agrees with its higher oxygen content in the elemental analysis (see Table 1). This finding could be related to the presence of a significant amount of K in the mineral fraction of the OSR700 biochar. As reported elsewhere, K may act as catalyst promoting the formation of surface oxygenated groups, in particular, those with carbonyl and hydroxyl functionalities (Zhao et al., 2016a). Therefore, the stronger elimination of oxygenated groups detected in low ash biochars would be counteracted in case there is a significant amount of potassium in the carbon matrix.

To corroborate this effect, the activated biochars were subjected to TPD-MS analyses. This technique allows to determine what kind of oxygenated functional groups are present on the carbon surface following the evolution of the release of CO, CO_2 and/or H_2O with the temperature (Bedia et al., 2018; Figueiredo and Pereira, 2010; Ishii and Kyotani, 2016). The spectra so obtained are displayed in Fig. 5. Thus, regarding the H_2O profile, OSR700 derived carbon presents an intense broad band (150–400 °C) with three maximums centred at 200, 275 and 325 °C, the latter being assigned to the chemisorbed water that would be evolved due to dehydration of neighbour hydroxyl groups, leading to the formation of the carboxylic anhydride, which decomposes to CO and CO_2 at higher temperatures (350–627 °C) (Ghouma et al., 2015; Otake and Jenkins, 1993; Shafeeyan et al., 2010). Then, in the CO desorption profile, this sample experiences an important increase at higher temperatures, being associated with carboxylic anhydrides (350–600 °C), phenol (600–700 °C), and especially to neutral or basic oxygenated functional groups: carbonyl and quinones (700–900 °C) (Shafeeyan et al., 2010; Shen et al., 2012).

Finally, regarding CO_2 desorption, this is related to acidic groups, and, in this case, it exhibits a broad desorption band with a maximum peak centred at 250 °C, along with a shoulder at 325 °C, which could be associated with the presence of carboxylic (150–400 °C) and lactone (200–600 °C) groups. There is an additional broad band (350–600 °C) that can be assigned to the carboxylic anhydride decomposition with a maximum peak centred at high temperature (600 °C) (Shafeeyan et al., 2010; Shen et al., 2012). These results clearly denote that OSR700-A900CO_2 presents a wide variety of oxygenated groups, being much higher than in the case of the OAK derived biochar. As was above

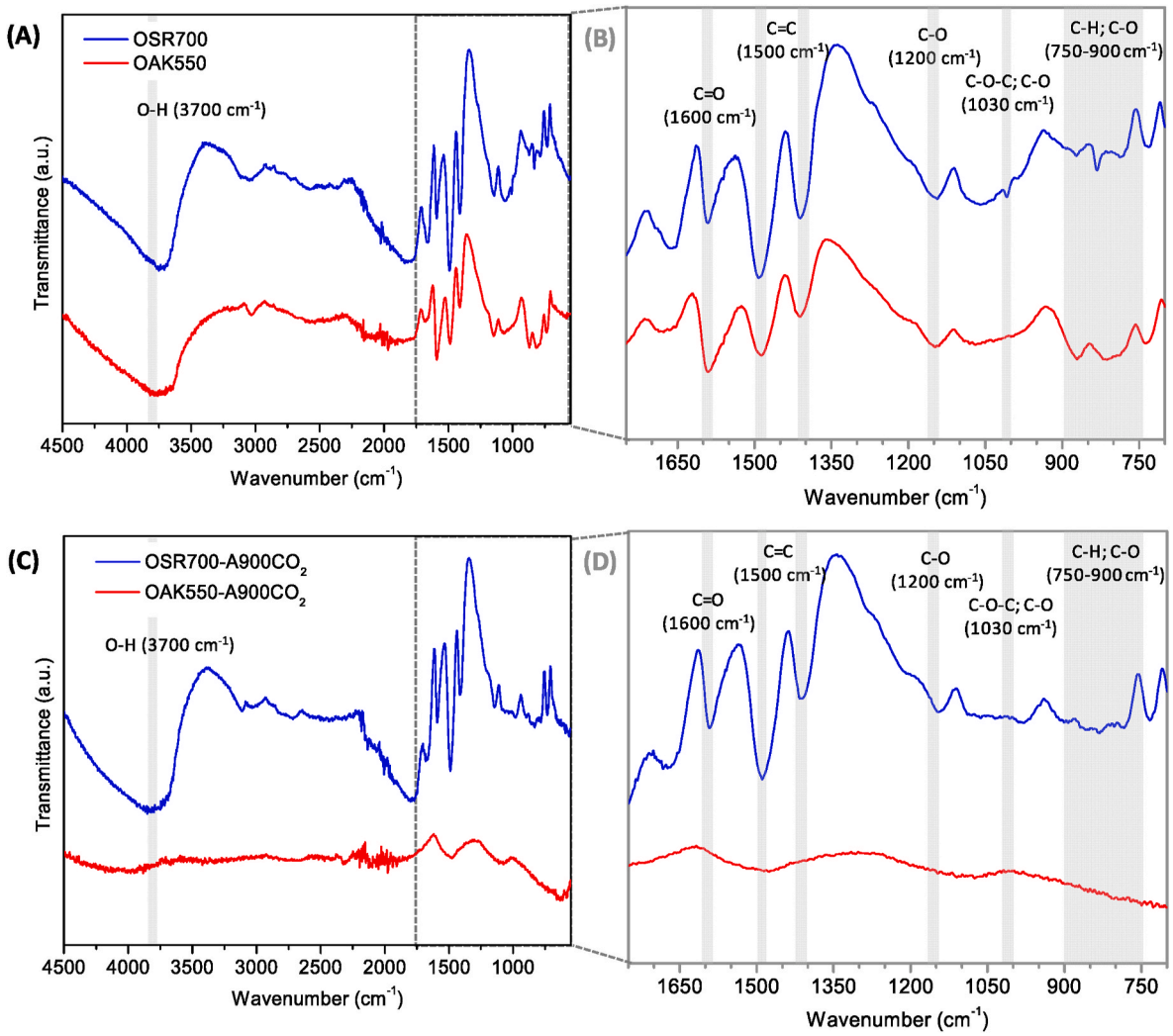

Fig. 4. FT-IR spectra of raw biochars (A, B) and derived activated carbons (C, D).

described, K may promote the formation of oxygenated moieties related to C–O bonds, which improves the NO removal performance of carbon materials (Wang et al., 2022; Zhao et al., 2016b) It is remarkable that activated biochars present a different relation between carboxylic and anhydride groups. In this respect, OSR700-A900CO_2 contains the same amount of both groups, while OAK550-A900CO_2 presents a lower proportion of carboxylic groups.

3.2. NO removal activity tests from polluted gaseous streams

After the activated carbons derived from different biochars were physico-chemically characterized, their performance on the NO elimination at low concentrations was evaluated. For that purpose, different experimental conditions, such as temperature, NO concentration, flue gas diluent (N_2 or air), and activated carbon load, were tested to investigate how they influence the NO removal efficiency and to assess which carbon features are more relevant in the oxidation/elimination process. First, blank tests consisting of passing N_2 or air flows containing NO through the unloaded filter, were carried out to assess if the oxidation of NO to NO_2 could take place in the gas phase under oxidizing atmospheres in absence of activated carbon. In these experiments, no variation was observed in the outlet NO concentration with respect to the initial, as well as negligible NO_2 concentrations, corroborating that the oxidation of NO to NO_2 is insignificant in the gas phase in the absence of solid carbon, which confirms previous results in the literature indicating the need of a solid catalyst to oxidize NO to NO_2 (Shen et al., 2016; Tsukahara et al., 1999).

3.2.1. Effect of temperature on the NO removal capacity from air streams

The effect of the temperature during the adsorption tests on the NO elimination capacity was evaluated under air flow. In this sense, Fig. 6 depicts the total NO removal capacity of activated biochars at 25, 50 and 75 °C as a function of the NO concentrations at the reactor inlet. The rise in the temperature enhances the NO removal efficiency of the OSR700-derived carbon by approximately 37%, achieving a complete elimination of NO when the experiment is performed at 50 °C. This significant improvement of the OSR700-A900CO_2 capacity could be derived from the considerable amount of oxygenated surface functionalities, which might be activated by temperature, promoting the NO to NO_2 oxidation that would remain easily adsorbed on the material surface. Moreover, in this case, when the temperature is slightly increased, the potassium contained in the mineral fraction could also promote the formation of surface C–O bonds, which increases the NO oxidation rate, leading to better NO removal efficiencies. A similar effect has been previously reported with coal-activated carbons doped with K traces and corroborated by DFT simulation (Wang et al., 2022). Nevertheless, to discard the catalytic activity of the mineral fraction in the NO oxidation process, an additional NO removal test was performed using an ash bed obtained from the combustion of the OSR700 activated carbon. In this experiment, NO removal was null, which confirms that NO oxidation is

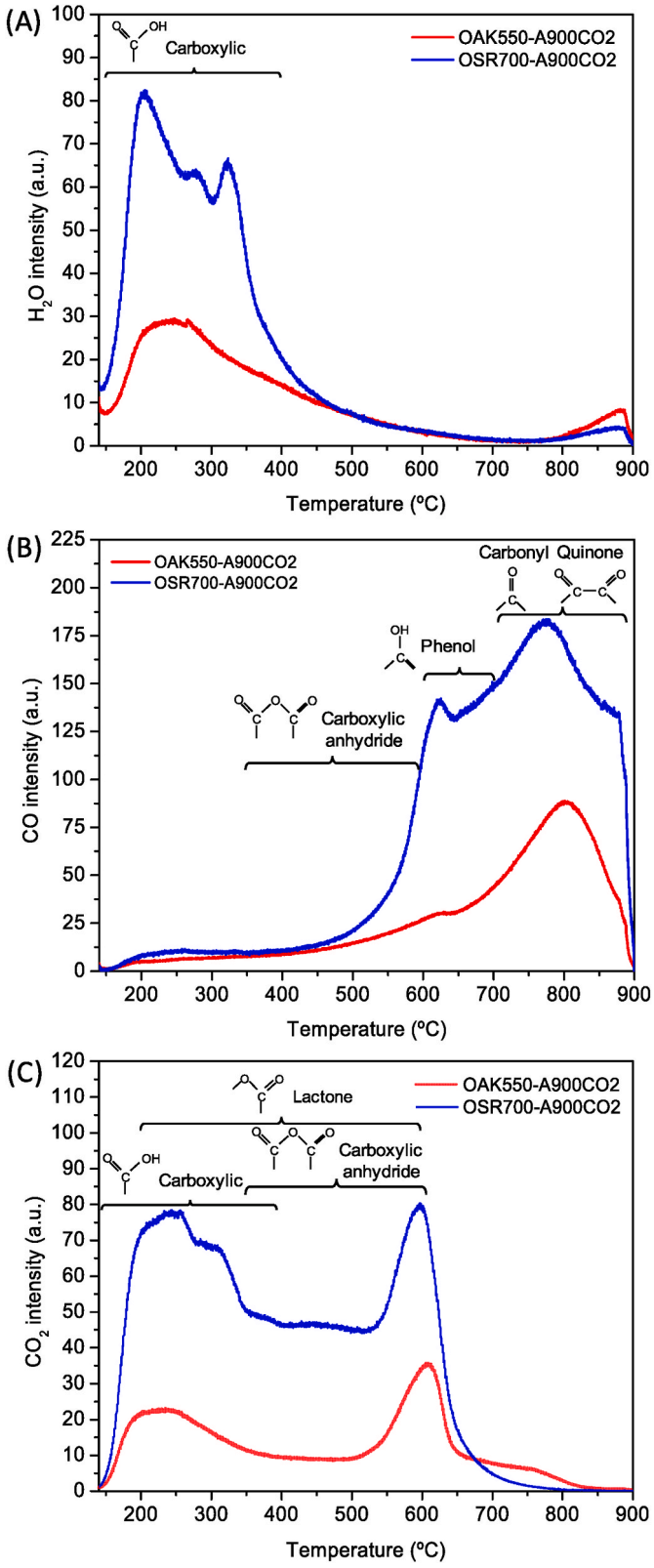

Fig. 5. H_2O (A), CO (B) and CO_2 (C) TPD-MS spectra of activated carbons derived from OSR700 and OAK550 biochars.

catalyzed by the surface active sites of the carbonaceous fraction of the biochar.

In contrast, OAK550-A900CO_2 leads to a complete removal of NO at 25 °C, being significantly higher than that exhibited by OSR700-derived

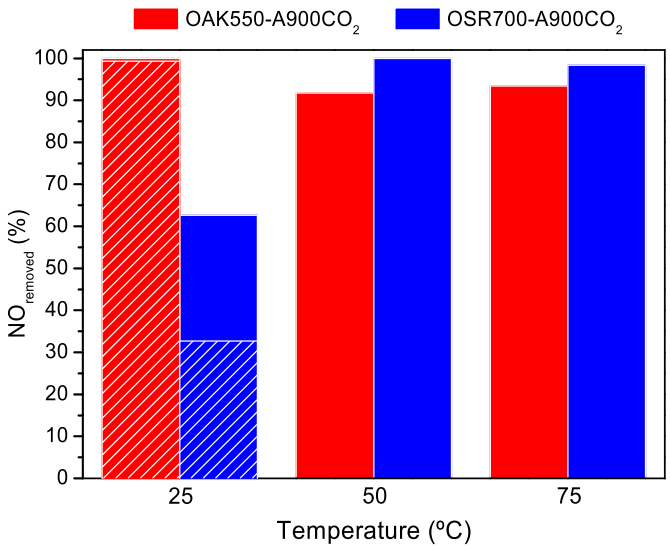

Fig. 6. Effect of the adsorption temperature on the NO removal capacity of activated carbons derived from OAK and OSR biochars under air flow. Experimental conditions: $[NO]_0$ = 5 ppmv; activated carbon bed: 3 g. Overlapped striped columns: 50 vol% RH in air flow.

activated biochar. However, its NO removal capacity decreased to some extent from 100 to 92–93% when the temperature increased up to 50 °C. This different behavior of both samples indicates that, at room temperature, NO removal process is favoured by the higher specific surface area and, especially, the narrower micropore size close to 6 Å of OAK550-A900CO_2. In this sense, considering that, before the oxidation itself, both NO and O_2 are initially co-adsorbed in the carbon micropores, these results suggest that, over the OAK activated biochar, the reactants co-adsorption step is the controlling stage, being unfavored at temperatures higher than the ambient.

Moreover, these carbons were also tested under humid air (50 vol% RH) at 25 °C, whose results are presented as overlapped striped columns in Fig. 6. Here, it can be observed that OSR-derived material presents a 47.8% loss of NO removal efficiency. This result might be linked to the higher proportion of oxygenated surface functional groups (see Fig. 5), due to water molecules associate to form clusters around those oxygen-containing functional groups, which may hinder pore entrance (De Ridder et al., 2012; Do et al., 2009; Nakamura et al., 2010), inhibiting partially the NO and O_2 interaction with the carbon surface. Thus, in the case of OAK-derived carbon, which possess very low proportion of oxygenated surface groups, the NO removal performance was hardly altered in presence of moisture, denoting that the more hydrophobic character of the carbon surface prevents the adsorption of water molecules on the active sites.

Therefore, it could be affirmed that OAK550-A900CO_2 would be a more convenient material for the removal of low concentrations of NO at room temperature and certain relative humidity, which are the typical conditions in semi-close spaces of urban areas.

3.2.2. Effect of NO concentration of polluted air streams and amount of carbon

The effect of the NO concentration (2.5–7.5 ppmv) in the air stream was also evaluated at 25 °C. Since the OAK550-derived sample achieved a full NO removal in the previous experiments (Fig. 7), and in order to appreciate more significant differences between both activated carbons, the amount of sample used in these assays was reduced to half (1.5 g). In this figure, the first observation is that reducing the carbon material to half caused a decrease of 36 and 40% in the removal capacity of both activated biochars with an NO inlet concentration of 5 ppmv. This means that the reduction of the carbon bed limits the contact time

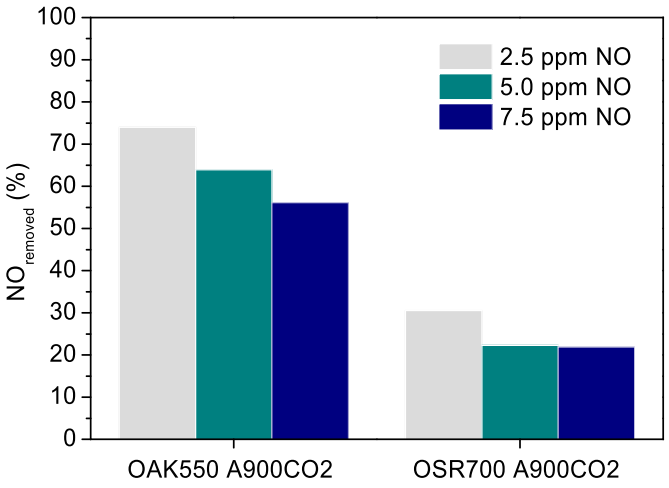

Fig. 7. NO removal capacity of activated carbons as a function of the NO concentration in the air stream. Experimental conditions: Temperature: 25 °C; carbon bed: 1.5 g.

between carbon and reactants (NO and O_2) hindering the complete removal of all the NO passing through. This effect occurs even employing half pollutant concentration (2.5 ppmv), at which none of the materials was able to fully remove the NO fed during the whole experiment. This effect was even more noticeable in the case of the OSR700 activated carbon. These results indicate that the process is more sensitive to the amount of carbon and, accordingly, to the contact time, when the adsorption process is chemically controlled by the interaction of oxygenated surface groups, as occurs in the OSR700-derived activated carbon. In this regard, if the NO removed percentages were estimated on an ash-free basis, taking into account just the amount of carbon in the sample, in all cases, the elimination capacity of OAK550-A900CO_2 was significantly higher.

3.2.3. Breakthrough curves and total NO removal capacity of activated carbons

Finally, the NO breakthrough curves at room temperature (25 °C) in air and nitrogen flue gas are shown in Fig. 8. Both activated carbons, regardless of their origin, show a much better NO removal capacity in air than in N_2 flow, which demonstrates the key role of the presence of oxygen in the gas phase to assist the oxidation of NO to NO_2 on active

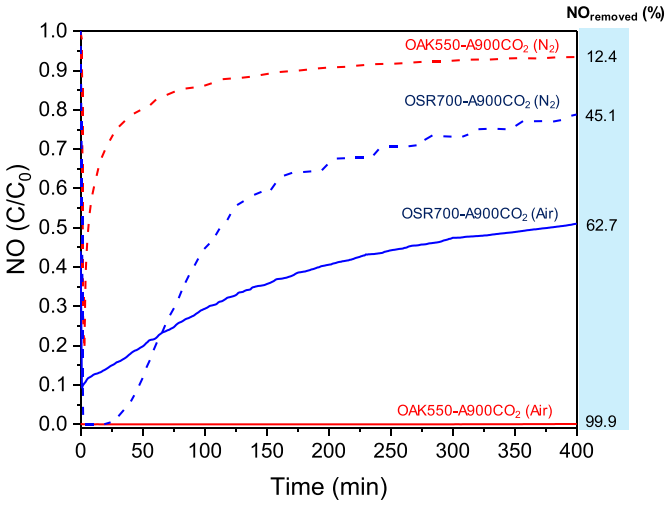

Fig. 8. Breakthrough curves of NO removal of activated carbons in air and N_2 flue gases. Experimental conditions: $[NO]_0$ = 5 ppmv; Temperature: 25 °C; carbon bed: 3 g.

sites of carbon materials as explained in a previous work (G. Diaz-Maroto et al., 2023). Important differences are observed between the two activated carbons in terms of NO removal along the time. In this regard, while OAK550-A900CO_2 was able to entirely remove the NO (99.9%) from the air flow during the 400 min of the test, the OSR700 activated carbon did not totally eliminate the NO from the start of the experiment, with C/C_0 values continuously increasing with time up to final values of 0.51, which was reflected in its quite inferior total removal capacity of 62.7%. This result could be related, as above discussed, to the higher S_{BET} area and, in particular, the narrower micropore size distribution of OAK550-A900CO_2. As it is previously mentioned, homogeneous micropores with sizes close to ~ 6–7 Å allow intimate contact between NO and O_2, which had molecular sizes of 0.317 nm and 0.346 nm, respectively, acting as nanoreactors for the NO oxidation process (Zhu et al., 2022).

The NO removal capacity gets much worse in absence of molecular oxygen in the gas stream, and in particular, in the case of OAK550-derived carbon. Thus, the activated carbons exhibit a very low NO removal efficiency in nitrogen flow, achieving C/C_0 values in the range of 0.6–0.9 at a time of 120 min. This fact suggests that, in the absence of oxygen, the oxygenated surface functional groups may assist the NO oxidation over carbons (Deng et al., 2020). Thus, OSR700-A900CO_2 shows better NO removal capacity in N_2 than in the other carbon. From these results, it can be envisaged that the NO removal process, in presence of oxygen, is controlled by the textural properties of the carbonaceous solid while, under nitrogen flow, is dominated by the chemical surface properties of the activated carbon, such as the oxygen functional groups.

4. Conclusions

In this study, the NO removal performance of two activated carbons (OSR700-A900CO_2 and OAK550-A900CO_2) was investigated at low concentrations (2.5–7.5 ppmv) and temperatures ranging from 25 to 75 °C. The textural properties and surface chemistry of the activated biochar, which strongly depends on their origin and ash content, are the most influential variables in the NO removal capacity. However, it was found that their impact is greatly conditioned by the temperature.

Thus, OSR700-A900CO_2 does not achieve a total NO elimination (62.7%) at room temperature, but it improves the NO removal capacity with the temperature until it reaches a full NO removal at 50 and 75 °C. These results denote that, at those temperatures, surface oxygenated functional groups, whose population is significantly higher in this sample, may favor the NO oxidation process. The role of the surface oxygenated groups is confirmed by the experiment performed in absence of oxygen, in which the NO removal performance of OSR700-A900CO_2 is better than that exhibited by the OAK activated biochar, although in both cases lower than those obtained in an oxidizing atmosphere. On the other hand, the presence of moisture in the air flow significantly decreased the NO removal performance of OSR700-derived sample due to the competition of water molecules with NO and O_2 by carbon surface functional groups. For the former sample, the generation of a meaningful proportion of oxygenated groups could be aided by its high ash content, very rich in K. In contrast, OAK550-A900CO_2 is the best carbon at room temperature, achieving a full NO elimination efficiency during the 400 min of the assay, even under humid air conditions. This result is attributed to its narrower microporosity centred at around 6 Å, which provides very close contact between NO and O_2, favoring the oxidation process in the carbon active sites. These promising results demonstrate the potential of activated biochars as low-cost and renewable carbons for the removal of NO at low concentrations and temperatures around the ambient, typical conditions of semi-closed environments of urban areas, such as parking lots and tunnels.

Credit author contribution statement

Carlos G. Díaz-Maroto: Methodology, Software, Formal analysis, Investigation, Writing – original draft, Visualization; **Ondřej Mašek**: biochar sample, review and editing; **Patricia Pizarro**: Writing – review and editing, Supervision; **David P. Serrano**: Writing – review and editing, Supervision; **Inés Moreno**: Conceptualization, Validation, Writing – review and editing, Supervision; **Javier Fermoso**: Conceptualization, Methodology, Validation, Writing – review and editing, Visualization, Supervision, Funding acquisition.

Declaration of competing interest

The authors declare that they have no known competing financial interests or personal relationships that could have appeared to influence the work reported in this paper.

Data availability

Data will be made available on request.

Acknowledgements

J. Fermoso gratefully acknowledges the financial support from the Comunidad de Madrid through the Talent Attraction Programme (2018-T1/AMB-10023).

Appendix A. Supplementary data

Supplementary data to this article can be found online at https://doi.org/10.1016/j.jenvman.2023.118031.

References

Adapa, S., Gaur, V., Verma, N., 2006. Catalytic oxidation of NO by activated carbon fiber (ACF). Chem. Eng. J. 116, 25–37. https://doi.org/10.1016/j.cej.2005.10.007.

Anthonysamy, S.I., Lahijani, P., Mohammadi, M., Mohamed, A.R., 2022. Dynamic adsorption of nitric oxide (NO) in a fixed-bed reactor using rubber seed shell-derived biochar. Biointerface Res. Appl. Chem. 12, 1638–1650. https://doi.org/10.33263/BRIAC122.16381650.

Armynah, B., Tahir, D., Tandilayuk, M., Djafar, Z., Piarah, W.H., 2019. Potentials of biochars derived from bamboo leaf biomass as energy sources: effect of temperature and time of heating. Int. J. Biomater. 2019, 12–18. https://doi.org/10.1155/2019/3526145.

Atkinson, J.D., Zhang, Z., Yan, Z., Rood, M.J., 2013. Evolution and impact of acidic oxygen functional groups on activated carbon fiber cloth during NO oxidation. Carbon N. Y. 54, 444–453. https://doi.org/10.1016/j.carbon.2012.11.060.

Azargohar, R., Dalai, A.K., 2006. Biochar as a precursor of activated carbon. Applied Biochemistry and Biotechnology. Twenty-Seventh Symp. Biotechnol. Fuels Chem. 131, 762–773. https://doi.org/10.1007/978-1-59745-268-7_62.

Barroso-Bogeat, A., Alexandre-Franco, M., Fernández-González, C., Gómez-Serrano, V., 2019. Activated carbon surface chemistry: changes upon impregnation with Al(III), Fe(III) and Zn(II)-metal oxide catalyst precursors from NO3− aqueous solutions. Arab. J. Chem. 12, 3963–3976. https://doi.org/10.1016/j.arabjc.2016.02.018.

Bedia, J., Peñas-Garzón, M., Gómez-Avilés, A., Rodriguez, J., Belver, C., 2018. A review on the synthesis and characterization of biomass-derived carbons for adsorption of emerging contaminants from water. Chimia 4, 63. https://doi.org/10.3390/c4040063.

Brandenberger, S., Kröcher, O., Tissler, A., Althoff, R., 2008. The state of the art in selective catalytic reduction of NOx by ammonia using metal-exchanged zeolite catalysts. Catal. Rev. - Sci. Eng. 50, 492–531. https://doi.org/10.1080/01614940802480122.

Chen, Y., Zhang, X., Chen, W., Yang, H., Chen, H., 2017. The structure evolution of biochar from biomass pyrolysis and its correlation with gas pollutant adsorption performance. Bioresour. Technol. 246, 101–109. https://doi.org/10.1016/j.biortech.2017.08.138.

De Ridder, D.J., Verliefde, A.R.D., Heijman, B.G.J., Gelin, S., Pereira, M.F.R., Rocha, R.P., Figueiredo, J.L., Amy, G.L., Van Dijk, H.C., 2012. A thermodynamic approach to assess organic solute adsorption onto activated carbon in water. Carbon N. Y. 50, 3774–3781. https://doi.org/10.1016/j.carbon.2012.03.052.

Demir, A., 2015. Investigation of air quality in the underground and aboveground multi-storey car parks in terms of exhaust emissions. Procedia - Soc. Behav. Sci. 195, 2601–2611. https://doi.org/10.1016/j.sbspro.2015.06.461.

Deng, W., Tao, C., Cobb, K., Zhou, H., Su, Y., Ruan, R., 2020. Catalytic oxidation of NO at ambient temperature over the chars from pyrolysis of sewage sludge. Chemosphere 251, 126429. https://doi.org/10.1016/j.chemosphere.2020.126429.

Derwent, R., Hjellbrekke, A.-G., 2019. Air Pollution by Ozone across Europe: Handbook of Environmental Chemistry. EEA. Report No 4/2012.

Do, D.D., Junpirom, S., Do, H.D., 2009. A new adsorption-desorption model for water adsorption in activated carbon. Carbon N. Y. 47, 1466–1473. https://doi.org/10.1016/j.carbon.2009.01.039.

Feng, S., Li, Z., Shen, B., Yuan, P., Ma, J., Wang, Z., Kong, W., 2022. An overview of the deactivation mechanism and modification methods of the SCR catalysts for denitration from marine engine exhaust. J. Environ. Manag. 317, 115457 https://doi.org/10.1016/j.jenvman.2022.115457.

Fermoso, J., Hernando, H., Jiménez-Sánchez, S., Lappas, A.A., Heracleous, E., Pizarro, P., Coronado, J.M., Serrano, D.P., 2017. Bio-oil production by lignocellulose fast-pyrolysis: isolating and comparing the effects of indigenous versus external catalysts. Fuel Process. Technol. 167, 563–574. https://doi.org/10.1016/j.fuproc.2017.08.009.

Figueiredo, J.L., Pereira, M.F.R., 2010. The role of surface chemistry in catalysis with carbons. Catal. Today 150, 2–7. https://doi.org/10.1016/j.cattod.2009.04.010.

G. Diaz-Maroto, C., Saenz de Miera, B., Collado, L., Fermoso, Jose, Masek, O., Pizarro, P., Serrano, D.P., Moreno, I., Fermoso, Javier, 2023. Removal of NO at low concentration from air in urban built environments by activated miscanthus biochar. J. Environ. Manag. 336, 117610 https://doi.org/10.1016/j.jenvman.2023.117610.

Ghouma, I., Jeguirim, M., Dorge, S., Limousy, L., Matei Ghimbeu, C., Ouederni, A., 2015. Activated carbon prepared by physical activation of olive stones for the removal of NO2 at ambient temperature. Compt. Rendus Chem. 18, 63–74. https://doi.org/10.1016/j.crci.2014.05.006.

Ghouma, I., Jeguirim, M., Sager, U., Limousy, L., Bennici, S., Däuber, E., Asbach, C., Ligotski, R., Schmidt, F., Ouederni, A., 2017. The potential of activated carbon made of agro-industrial residues in NOx immissions abatement. Energies 10, 1508. https://doi.org/10.3390/en10101508.

Gui, R., Yan, Q., Xue, T., Gao, Y., Li, Y., Zhu, T., Wang, Q., 2022. The promoting/inhibiting effect of water vapor on the selective catalytic reduction of NOx. J. Hazard Mater. 439, 129665 https://doi.org/10.1016/j.jhazmat.2022.129665.

Gwenzi, W., Chaukura, N., Wenga, T., Mtisi, M., 2021. Biochars as media for air pollution control systems: contaminant removal, applications and future research directions. Sci. Total Environ. 753, 142249 https://doi.org/10.1016/j.scitotenv.2020.142249.

Hong, Z., Wang, Z., Li, X., 2017. Catalytic oxidation of nitric oxide (NO) over different catalysts: an overview. Catal. Sci. Technol. 7, 3440–3452. https://doi.org/10.1039/c7cy00760d.

Hu, Q., Yang, H., Wu, Z., Lim, C.J., Bi, X.T., Chen, H., 2019. Experimental and modeling study of potassium catalyzed gasification of woody char pellet with CO2. Energy 171, 678–688. https://doi.org/10.1016/j.energy.2019.01.050.

Hwang, H., Sahin, O., Choi, J.W., 2017. Manufacturing a super-active carbon using fast pyrolysis char from biomass and correlation study on structural features and phenol adsorption. RSC Adv. 7, 42192–42202. https://doi.org/10.1039/c7ra06910c.

Ishii, T., Kyotani, T., 2016. Temperature Programmed Desorption, Materials Science and Engineering of Carbon. Tsinghua University Press Limited. https://doi.org/10.1016/b978-0-12-805256-3.00014-3.

Jagiello, J., Kenvin, J., Celzard, A., Fierro, V., 2019. Enhanced resolution of ultra micropore size determination of biochars and activated carbons by dual gas analysis using N2 and CO2 with 2D-NLDFT adsorption models. Carbon N. Y. 144, 206–215. https://doi.org/10.1016/j.carbon.2018.12.028.

Janu, R., Mrlik, V., Ribitsch, D., Hofman, J., Sedláček, P., Bielská, L., Soja, G., 2021. Biochar surface functional groups as affected by biomass feedstock, biochar composition and pyrolysis temperature. Carbon Resour. Convers. 4, 36–46. https://doi.org/10.1016/j.crcon.2021.01.003.

Jeguirim, M., Belhachemi, M., Limousy, L., Bennici, S., 2018. Adsorption/reduction of nitrogen dioxide on activated carbons: textural properties versus surface chemistry – a review. Chem. Eng. J. 347, 493–504. https://doi.org/10.1016/j.cej.2018.04.063.

Jouiad, M., Al-Nofeli, N., Khalifa, N., Benyettou, F., Yousef, L.F., 2015. Characteristics of slow pyrolysis biochars produced from rhodes grass and fronds of edible date palm. J. Anal. Appl. Pyrolysis 111, 183–190. https://doi.org/10.1016/j.jaap.2014.10.024.

Kalinke, C., Oliveira, P.R., Oliveira, G.A., Mangrich, A.S., Marcolino-Junior, L.H., Bergamini, M.F., 2017. Activated biochar: preparation, characterization and electroanalytical application in an alternative strategy of nickel determination. Anal. Chim. Acta 983, 103–111. https://doi.org/10.1016/j.aca.2017.06.025.

Lozano-Castelló, D., Cazorla-Amorós, D., Linares-Solano, A., 2004. Usefulness of CO2 adsorption at 273 K for the characterization of porous carbons. Carbon N. Y. 42, 1233–1242. https://doi.org/10.1016/j.carbon.2004.01.037.

Lu, P., Huang, Q., Chi, Y., Yan, J., 2017. Preparation of high catalytic activity biochar from biomass waste for tar conversion. J. Anal. Appl. Pyrolysis 127, 47–56. https://doi.org/10.1016/j.jaap.2017.09.003.

Mašek, O., Buss, W., Roy-Poirier, A., Lowe, W., Peters, C., Brownsort, P., Mignard, D., Pritchard, C., Sohi, S., 2018. Consistency of biochar properties over time and production scales: a characterisation of standard materials. J. Anal. Appl. Pyrolysis 132, 200–210. https://doi.org/10.1016/j.jaap.2018.02.020.

Mochida, I., Kisamori, S., Hironaka, M., Kawano, S., Matsumura, Y., Yoshikawa, M., 1994. Oxidation of NO into NO2 over active carbon fibers. Energy Fuel. 8, 1341–1344. https://doi.org/10.1021/ef00048a024.

Mochida, I., Kawabuchi, Y., Kawano, S., Matsumura, Y., Yoshikawa, M., 1997. High catalytic activity of pitch-based activated carbon fibres of moderate surface area for oxidation of NO to NO2 at room temperature. Fuel 76, 543–548. https://doi.org/10.1016/S0016-2361(96)00223-2.

Nakamura, M., Ohba, T., Branton, P., Kanoh, H., Kaneko, K., 2010. Equilibration-time and pore-width dependent hysteresis of water adsorption isotherm on hydrophobic microporous carbons. Carbon N. Y. 48, 305–308. https://doi.org/10.1016/j.carbon.2009.09.008.

Nor, N.M., Chung, L.L., Teong, L.K., Mohamed, A.R., 2013. Synthesis of activated carbon from lignocellulosic biomass and its applications in air pollution control — a review. Biochem. Pharmacol. 1, 658–666. https://doi.org/10.1016/j.jece.2013.09.017.

Otake, Y., Jenkins, R.G., 1993. Characterization of oxygen-containing surface complexes created on a microporous carbon by air and nitric acid treatment. Carbon N. Y. 31, 109–121. https://doi.org/10.1016/0008-6223(93)90163-5.

Pan, L., Zhou, X., Zhao, H., Wan, G., Li, Q., Wang, N., Huang, W., Chen, H., 2017. Nanoflower-like Mg-doped MnOx for facile removal of low-concentration NOx at room temperature. Catal. Commun. 97, 70–73. https://doi.org/10.1016/j.catcom.2017.04.020.

Qiu, H., Lv, L., Pan, B.C., Zhang, Q.J., Zhang, W.M., Zhang, Q.X., 2009. Critical review in adsorption kinetic models. J. Zhejiang Univ. - Sci. 10, 716–724. https://doi.org/10.1631/jzus.A0820524.

Qu, J., Wang, Y., Tian, X., Jiang, Z., Deng, F., Tao, Y., Jiang, Q., Wang, L., Zhang, Y., 2021. KOH-activated porous biochar with high specific surface area for adsorptive removal of chromium (VI) and naphthalene from water: affecting factors, mechanisms and reusability exploration. J. Hazard Mater. 401, 123292 https://doi.org/10.1016/j.jhazmat.2020.123292.

Shafeeyan, M.S., Daud, W.M.A.W., Houshmand, A., Shamiri, A., 2010. A review on surface modification of activated carbon for carbon dioxide adsorption. J. Anal. Appl. Pyrolysis 89, 143–151. https://doi.org/10.1016/j.jaap.2010.07.006.

Shaw, S., Van Heyst, B., 2022. An evaluation of risk ratios on physical and mental health correlations due to increases in ambient nitrogen oxide (NOx) concentrations. Atmosphere (Basel) 13. https://doi.org/10.3390/atmos13060967.

Shen, W., Li, Z., Liu, Y., 2012. Surface chemical functional groups modification of porous carbon. Recent Pat. Chem. Eng. 1, 27–40. https://doi.org/10.2174/2211334710801010027.

Shen, Y., Ge, X., Chen, M., 2016. Catalytic oxidation of nitric oxide (NO) with carbonaceous materials. RSC Adv. 6, 8469–8482. https://doi.org/10.1039/c5ra24148k.

Shu, Z., Chen, Y., Huang, W., Cui, X., Zhang, L., Chen, H., Zhang, G., Fan, X., Wang, Y., Tao, G., He, D., Shi, J., 2013. Room-temperature catalytic removal of low-concentration NO over mesoporous Fe-Mn binary oxide synthesized using a template-free approach. Appl. Catal. B Environ. 140–141, 42–50. https://doi.org/10.1016/j.apcatb.2013.03.030.

Siipola, V., Tamminen, T., Källi, A., Lahti, R., Romar, H., Rasa, K., Keskinen, R., Hyväluoma, J., Hannula, M., Wikberg, H., 2018. Effects of biomass type, carbonization process, and activation method on the properties of bio-based activated carbons. Bioresources 13, 5976–6002.

Silas, K., Ghani, W.A.W.A.K., Choong, T.S.Y., Rashid, U., 2019. Carbonaceous materials modified catalysts for simultaneous SO2/NOx removal from flue gas: a review. Catal. Rev. - Sci. Eng. 61, 134–161. https://doi.org/10.1080/01614940.2018.1482641.

Thommes, M., Kaneko, K., Neimark, A.V., Olivier, J.P., Rodriguez-Reinoso, F., Rouquerol, J., Sing, K.S.W., 2015. Physisorption of gases, with special reference to the evaluation of surface area and pore size distribution (IUPAC Technical Report). Pure Appl. Chem. 87, 1051–1069. https://doi.org/10.1515/pac-2014-1117.

Tsukahara, H., Ishida, T., Mayumi, M., 1999. Gas-phase oxidation of nitric oxide: chemical kinetics and rate constant. Nitric Oxide - Biol. Chem. 3, 191–198. https://doi.org/10.1006/niox.1999.0232.

Valenciano, R., Aylón, E., Izquierdo, M.T., 2015. A critical short review of equilibrium and kinetic adsorption models for vocs breakthrough curves modelling. Adsorpt. Sci. Technol. 33, 851–870. https://doi.org/10.1260/0263-6174.33.10.851.

Wang, M.X., Huang, Z.H., Shimohara, T., Kang, F., Liang, K., 2011. NO removal by electrospun porous carbon nanofibers at room temperature. Chem. Eng. J. 170, 505–511. https://doi.org/10.1016/j.cej.2011.01.017.

Wang, J., Zhu, J., Zhou, X., Du, Y., Huang, W., Liu, J., Zhang, W., Shi, J., Chen, H., 2015. Nanoflower-like weak crystallization manganese oxide for efficient removal of low-concentration NO at room temperature. J. Mater. Chem. 3, 7631–7638. https://doi.org/10.1039/c5ta00468c.

Wang, M.R., Wang, L.Y., Zhang, X.Y., Cheng, X.X., Wang, Z.Q., 2022. Influence mechanism of trace K element on NOx adsorption of coal-based carbon materials at low temperature. J. Fuel Chem. Technol. 50, 884–895. https://doi.org/10.1016/S1872-5813(21)60199-8.

Yang, R., Liu, G., Li, M., Zhang, J., Hao, X., 2012. Preparation and N_2, CO_2 and H_2 adsorption of super activated carbon derived from biomass source hemp (Cannabis sativa L.) stem. Microporous Mesoporous Mater. 158, 108–116. https://doi.org/10.1016/j.micromeso.2012.03.004.

Zhang, W.J., Rabiei, S., Bagreev, A., Zhuang, M.S., Rasouli, F., 2008. Study of NO adsorption on activated carbons. Appl. Catal. B Environ. 83, 63–71. https://doi.org/10.1016/j.apcatb.2008.02.003.

Zhang, Y.J., Xing, Z.J., Duan, Z.K., Li, M., Wang, Y., 2014. Effects of steam activation on the pore structure and surface chemistry of activated carbon derived from bamboo waste. Appl. Surf. Sci. 315, 279–286. https://doi.org/10.1016/j.apsusc.2014.07.126.

Zhao, J., Xia, Y., Li, M., Li, S., Li, W., Zhang, S., 2016a. A biophysicochemical model for NO removal by the chemical absorption-biological reduction integrated process. Environ. Sci. Technol. 50, 8705–8712. https://doi.org/10.1021/acs.est.6b01414.

Zhao, Y., Wang, H., Wang, T., 2016b. Adsorption of NO from flue gas by molecularly imprinted adsorbents. Chem. Eng. J. 306, 832–839. https://doi.org/10.1016/j.cej.2016.08.023.

Zhu, X., Zhang, L., Wang, T., Li, J., Zhou, X., Ma, C., Dong, Y., 2022. An updated study on NO catalytic oxidation over activated carbon: the effect of pore structure and a dual-site mechanism. Fuel 311, 122627. https://doi.org/10.1016/j.fuel.2021.122627.